Science Advances
AAAS

advances.sciencemag.org/cgi/content/full/5/12/eaay1211/DC1

Supplementary Materials for

Focusing light inside live tissue using reversibly switchable bacterial phytochrome as a genetically encoded photochromic guide star

Jiamiao Yang, Lei Li, Anton A. Shemetov, Sangjun Lee, Yuan Zhao, Yan Liu, Yuecheng Shen, Jingwei Li, Yuki Oka, Vladislav V. Verkhusha*, Lihong V. Wang*

*Corresponding author. Email: vladislav.verkhusha@einstein.yu.edu (V.V.V.); lvw@caltech.edu (L.V.W.)

Published 11 December 2019, *Sci. Adv.* **5**, eaay1211 (2019)
DOI: 10.1126/sciadv.aay1211

The PDF file includes:

Other Supplementary Material for this manuscript includes the following:

(available at advances.sciencemag.org/cgi/content/full/5/12/eaay1211/DC1)

Note S1. Frequency shifting of the tagged photons.

As shown in Fig. 1C, the GePGS was illuminated by 637-nm and 780-nm light alternatingly at a frequency f_{mod} of 20 Hz. In each cycle, the absorption coefficient of the GePGS at 780 nm, as a function of time t, can be express as

$$\mu_{\mathrm{a}}(t) = \begin{cases} a_1 - b_1\exp(-t/\tau_1), & 0 \le t < t_1, \text{ switching on} \\ a_2 + b_2\exp[-(t - t_1)/\tau_2], & t_1 \le t < t_2, \text{ switching off} \end{cases} \tag{S1}$$

where a_1, b_1, a_2 and b_2 are positive constants, τ_1 is the rise time of the switching on process, τ_2 is the fall time of the switching off process, $t_1 = 24$ ms is the duration of the switching on process, and $t_2 = 50$ ms is the duration of the whole cycle. Thus, the optical field of the 780-nm light passing through the GePGS was modulated by $\mu_{\mathrm{a}}(t)$ as

$$E_{\mathrm{mod}}(t) = A\exp\left(-\mu_{\mathrm{a}}(t)L/2\right)\cdot\exp\left[i\left(-2\pi f_0 t + \varphi_0\right)\right] \tag{S2}$$

where f_0 is the frequency of 780-nm light, A and φ_0 are the initial amplitude and phase of the 780-nm light, respectively, and L is the thickness of the GePGS. Because $\exp\left(-\mu_{\mathrm{a}}(t)L/2\right)$ is a periodic function with a fundamental frequency of f_{m}, Eq. (S2) can be expanded into a Fourier series

$$\begin{aligned} E_{\mathrm{mod}}(t) = {} & \sum_{n=1}^{\infty} AB_{-n}\exp\left\{i\left[-2\pi\left(f_0 - nf_{\mathrm{mod}}\right)t + \varphi_0\right]\right\} \\ & + \sum_{n=1}^{\infty} AB_n\exp\left\{i\left[-2\pi\left(f_0 + nf_{\mathrm{mod}}\right)t + \varphi_0\right]\right\} \\ & + AB_0\exp\left[i\left(-2\pi f_0 t + \varphi_0\right)\right] \end{aligned} \tag{S3}$$

where $n = 1, 2, 3, \cdots$, and

$$B_n = f_{\mathrm{mod}}\int_0^{1/f_{\mathrm{mod}}}\exp\left(-\mu_{\mathrm{a}}(t)L/2\right)\exp\left(i2\pi n f_{\mathrm{mod}}t\right)dt \tag{S4}$$

Thus, a portion of the 780-nm photons passing through the GePGS was shifted to frequencies of $f_0 \pm nf_{\mathrm{mod}}$. Here, we are interested in the components with the shifted frequencies of $-f_{\mathrm{mod}}$ and f_{mod}, which have the largest amplitudes among all the harmonics.

Note S2. Mathematical description of GePGS-guided optical focusing inside scattering media.

To mathematically describe the whole digital wavefront shaping process, all the optical fields are expressed by column vectors. The optical field $\mathbf{E}_{\mathrm{mod}}$ on the plane right after GePGS is decomposed into three components with the shifted frequencies of $-f_{\mathrm{mod}}$, 0, and f_{mod}, which are the components with the largest amplitudes, and the other higher order components are neglected. Thus, $\mathbf{E}_{\mathrm{mod}} = \mathbf{E}_{-1} + \mathbf{E}_0 + \mathbf{E}_{+1}$, where $\mathbf{E}_0$ is the unmodulated component, and $\mathbf{E}_{-1}$ and $\mathbf{E}_{+1}$ are the components modulated by the GePGS with shifted frequencies of $-f_{\mathrm{mod}}$ and f_{mod}, respectively. Each component contains J complex elements. For simplicity but without losing generality, among all the J elements in $\mathbf{E}_{-1}$ and $\mathbf{E}_{+1}$, we assume that the first element is the optical field where the GePGS is, and the rest of the elements are zeros, as shown below

$$\mathbf{E}_{-1} = (E_{-1}, 0, \ldots, 0)^T_{J\times 1} \tag{S5}$$

and

$$\mathbf{E}_{+1} = (E_{+1}, 0, \ldots, 0)^T_{J\times 1} \tag{S6}$$

where "T" stands for the transpose operator. According to Eq. (S3), E_{-1} and E_{+1} can be expressed as

$$E_{-1} = AB_{-1}\exp\{i[-2\pi(f_0 - f_{\mathrm{mod}})t + \varphi_0]\} \tag{S7}$$

and

$$E_{+1} = AB_{+1}\exp\{i[-2\pi(f_0 + f_{\mathrm{mod}})t + \varphi_0]\} \tag{S8}$$

According to Eq. (S4), B_{-1} and B_{+1} are complex conjugate, and can be expressed as $B\cdot\exp(-i\varphi_b)$ and $B\cdot\exp(i\varphi_b)$, respectively.

When $\mathbf{E}_{mod}$ propagates through a scattering medium described by a transmission matrix $\mathbf{T}$ and reaches a camera, the optical field $\mathbf{E}_{out}$ on the camera can be written as

$$\mathbf{E}_{out} = \mathbf{T}\cdot\mathbf{E}_{mod} = \mathbf{T}\cdot(\mathbf{E}_{-1} + \mathbf{E}_0 + \mathbf{E}_{+1}) \tag{S9}$$

where $\mathbf{T}$ is an $M\times J$ complex matrix whose element $t_{mj} = C_{mj}\exp\left(i\varphi_{mj}\right)$, $m = 1, \ldots, M, j = 1, \ldots, J$, follows a circular Gaussian distribution, and $\mathbf{E}_{out}$ is a column vector of M elements. The m-th element of $\mathbf{E}_{out}$ is $E_{out}^{(m)} = E_{TE}^{(m)} + E_{TE0}^{(m)}$, where $E_{TE}^{(m)}$ and $E_{TE0}^{(m)}$ are the m-th element of $\mathbf{T}\cdot(\mathbf{E}_{-1} + \mathbf{E}_{+1})$ and $\mathbf{T}\cdot\mathbf{E}_0$, respectively. Assume that the reference beam is a plane wave, all the elements of its optical field $\mathbf{E}_{ref}$ have the same expression of $E_{ref} = A_{ref}\exp[i(-2\pi f_0 t + \varphi_{ref})]$, where A_{ref} and φ_{ref} denote the amplitude and initial phase, respectively. When $\mathbf{E}_{out}$ and $\mathbf{E}_{ref}$ interfere with each other, a hologram is formed and its m-th element is

$$\begin{aligned} I_{inter}^{(m)} &= \left(E_{TE}^{(m)} + E_{TE0}^{(m)} + E_{ref}\right)\times\left(E_{TE}^{(m)} + E_{TE0}^{(m)} + E_{ref}\right)^* \\ &= E_{TE}^{(m)}E_{TE}^{(m)*} + E_{ref}E_{ref}^* + E_{TE0}^{(m)}E_{TE0}^{(m)*} \\ &\quad +2\mathrm{real}\left(E_{TE}^{(m)}E_{ref}^* + E_{TE}^{(m)}E_{TE0}^{(m)*} + E_{ref}E_{TE0}^{(m)*}\right) \end{aligned} \tag{S10}$$

where real(·) denotes the real part of a complex number. By differentiating the two holograms at time $1/(4f_{mod})$ and $3/(4f_{mod})$ and eliminating the components that do not change over time, the m-th element of the differential hologram is obtained as

$$\begin{aligned} \Delta I_{inter}^{(m)} &= I_{inter}^{(m)}\Big|_{t=1/(4f_{mod})} - I_{inter}^{(m)}\Big|_{t=3/(4f_{mod})} \\ &= 2\mathrm{real}\left(E_{TE}^{(m)}E_{ref}^* + E_{TE}^{(m)}E_{TE0}^{(m)*}\right)\Big|_{t=1/(4f_{mod})} \\ &\quad - 2\mathrm{real}\left(E_{TE}^{(m)}E_{ref}^* + E_{TE}^{(m)}E_{TE0}^{(m)*}\right)\Big|_{t=3/(4f_{mod})} \end{aligned} \tag{S11}$$

Because the amplitude of E_{ref} is much larger than that of $E_{\mathrm{TE0}}^{(m)}$ in our experiments, $E_{\mathrm{TE}}^{(m)} E_{\mathrm{TE0}}^{(m)*}$ is also neglected; thus, Eq. (S11) can be simplified to

$$\Delta I_{\mathrm{inter}}^{(m)} = 2\mathrm{real}\left(E_{\mathrm{TE}}^{(m)} E_{\mathrm{ref}}^{*}\right)\Big|_{t=1/(4f_{\mathrm{mod}})} - 2\mathrm{real}\left(E_{\mathrm{TE}}^{(m)} E_{\mathrm{ref}}^{*}\right)\Big|_{t=3/(4f_{\mathrm{mod}})} \tag{S12}$$

According to Eqs. (S5–S9), we obtain

$$\begin{aligned} E_{\mathrm{TE}}^{(m)} &= ABt_{m1}\exp(i\varphi_0)\left(\exp\{i[-2\pi(f_0 - f_{\mathrm{mod}})t - \varphi_{\mathrm{b}}]\}\right. \\ &\quad \left.+\exp\{i[-2\pi(f_0 + f_{\mathrm{mod}})t + \varphi_{\mathrm{b}}]\}\right) \\ &= ABC_{m1}\exp[i(\varphi_{m1} + \varphi_0)]\left(\exp\{i[-2\pi(f_0 - f_{\mathrm{mod}})t - \varphi_{\mathrm{b}}]\}\right. \\ &\quad \left.+\exp\{i[-2\pi(f_0 + f_{\mathrm{mod}})t + \varphi_{\mathrm{b}}]\}\right) \end{aligned} \tag{S13}$$

By substituting Eq. (S13) into Eq. (S12), the m-th element of the differential hologram can be expressed as

$$\Delta I_{\mathrm{inter}}^{(m)} = 4ABC_{m1}A_{\mathrm{ref}}\cos(\varphi_{m1} + \varphi_0 - \varphi_{\mathrm{ref}})\sin(\varphi_{\mathrm{b}}) \tag{S14}$$

We define a binary amplitude map $\mathbf{D}_{\mathrm{DMD}}$ by thresholding $\Delta I_{\mathrm{inter}}^{(m)}$ at 0, whose m-th element is

$$D_{\mathrm{DMD}}^{(m)} = \begin{cases} 1, & \Delta I_{\mathrm{inter}}^{(m)} \geq 0 \\ 0, & \Delta I_{\mathrm{inter}}^{(m)} < 0 \end{cases} \tag{S15}$$

In the wavefront playback step, this binary amplitude map $\mathbf{D}_{\mathrm{DMD}}$ is displayed on a DMD to modulate the reference beam. When the modulated beam passes back through the scattering medium, the optical field on the plane of the GePGS is $\mathbf{E}_{\mathrm{back}} = A_{\mathrm{ref}}\exp(i\varphi_{\mathrm{ref}})\mathbf{T}^{T} \cdot \mathbf{D}_{\mathrm{DMD}}$, whose j-th element is

$$
\begin{aligned}
E_{\text{back}}^{(j)} &= A_{\text{ref}}\exp\left(i\varphi_{\text{ref}}\right)\sum_{m=1}^{M} t_{mj} D_{\text{DMD}}^{(m)} \\
&= A_{\text{ref}}\exp\left(i\varphi_{\text{ref}}\right)\sum_{m=1}^{M} C_{mj}\exp\left(i\varphi_{mj}\right) D_{\text{DMD}}^{(m)}
\end{aligned}
\tag{S16}
$$

We assume that $\sin\left(\varphi_{\text{b}}\right) > 0$ in Eq. (S14). From Eqs. (S14–S16), when $D_{\text{DMD}}^{(m)} = 1$, for the position where $j = 1$, the value φ_{mj} distributes uniformly in a range of $\left(-\pi/2 + \varphi_{\text{ref}} - \varphi_0,\ \pi/2 + \varphi_{\text{ref}} - \varphi_0\right)$, which means photons constructively interfere and thus form a bright focus on the GePGS; for positions where $j \neq 1$, φ_{mj} distributes uniformly in the whole phase space of $(0, 2\pi]$, which means that photons randomly interfere with each other and form a speckle background outside the GePGS.

Note S3. Minimizing the impact of the fast motions in scattering media.

During the process of OPC, both the GePGS and the fast decorrelation components, such as blood flow and respiration motions, can tag photons. Consequently, the fast decorrelation components and the GePGS complete for light focusing. When fast decorrelation components exist, $E_{\text{TE0}}^{(m)}$ can be decomposed into two parts, $E_{\text{TE0}}^{(m)} = E_{\text{TES}}^{(m)} + E_{\text{TED}}^{(m)}$, where $E_{\text{TES}}^{(m)}$ is the stable component that does not change during the OPC process and $E_{\text{TED}}^{(m)}$ is the fast decorrelation component that varies during this process. Thus, Eq. (S10) can be rewritten as

$$
\begin{aligned}
I_{\text{inter}}^{(m)} &= \left(E_{\text{TE}}^{(m)} + E_{\text{TES}}^{(m)} + E_{\text{TED}}^{(m)} + E_{\text{ref}}\right) \times \left(E_{\text{TE}}^{(m)} + E_{\text{TES}}^{(m)} + E_{\text{TED}}^{(m)} + E_{\text{ref}}\right)^{*} \\
&= E_{\text{TE}}^{(m)} E_{\text{TE}}^{(m)*} + E_{\text{ref}} E_{\text{ref}}^{*} + E_{\text{TES}}^{(m)} E_{\text{TES}}^{(m)*} + E_{\text{TED}}^{(m)} E_{\text{TED}}^{(m)*} + 2\text{real}\Big(E_{\text{TE}}^{(m)} E_{\text{TES}}^{(m)*} \\
&\quad + E_{\text{TE}}^{(m)} E_{\text{TED}}^{(m)*} + E_{\text{TE}}^{(m)} E_{\text{ref}}^{*} + E_{\text{TES}}^{(m)} E_{\text{TED}}^{(m)*} + E_{\text{TES}}^{(m)} E_{\text{ref}}^{*} + E_{\text{TED}}^{(m)} E_{\text{ref}}^{*}\Big)
\end{aligned}
\tag{S17}
$$

By averaging the holograms at time points of $1/\left(4f_{\text{mod}}\right), 5/\left(4f_{\text{mod}}\right), \cdots, (4N-3)/\left(4f_{\text{mod}}\right)$, and time points of $3/\left(4f_{\text{mod}}\right), 7/\left(4f_{\text{mod}}\right), \cdots, (4N-1)/\left(4f_{\text{mod}}\right)$, respectively, we obtain two averaged holograms with a time interval of $1/\left(2f_{\text{mod}}\right)$. By differentiating these two averaged holograms and eliminating the components that do not change over time, the m-th element of the differential hologram is obtained as

$$\begin{aligned}\Delta\bar{I}_{\text{inter}}^{(m)} &= \frac{\sum_{n=1}^{N}\left[I_{\text{inter}}^{(m)}\big|_{t=(4n-3)/(4f_{\text{mod}})}\right]}{N} - \frac{\sum_{n=1}^{N}\left[I_{\text{inter}}^{(m)}\big|_{t=(4n-1)/(4f_{\text{mod}})}\right]}{N} \\ &= \frac{\sum_{n=1}^{N}\left[2\text{real}\left(E_{\text{TE}}^{(m)}E_{\text{TES}}^{(m)*}+E_{\text{TE}}^{(m)}E_{\text{TED}}^{(m)*}+E_{\text{TE}}^{(m)}E_{\text{ref}}^{*}+E_{\text{TES}}^{(m)}E_{\text{TED}}^{(m)*}+E_{\text{TED}}^{(m)}E_{\text{ref}}^{*}\right)\big|_{t=(4n-3)/(4f_{\text{mod}})}\right]}{N} \\ &\quad - \frac{\sum_{n=1}^{N}\left[2\text{real}\left(E_{\text{TE}}^{(m)}E_{\text{TES}}^{(m)*}+E_{\text{TE}}^{(m)}E_{\text{TED}}^{(m)*}+E_{\text{TE}}^{(m)}E_{\text{ref}}^{*}+E_{\text{TES}}^{(m)}E_{\text{TED}}^{(m)*}+E_{\text{TED}}^{(m)}E_{\text{ref}}^{*}\right)\big|_{t=(4n-1)/(4f_{\text{mod}})}\right]}{N}\end{aligned} \tag{S18}$$

Because the amplitude of E_{ref} is much larger than those of $E_{\text{TE}}^{(m)}$, $E_{\text{TES}}^{(m)}$ and $E_{\text{TED}}^{(m)}$ in our experiments, $E_{\text{TE}}^{(m)}E_{\text{TES}}^{(m)*}$ and $E_{\text{TE}}^{(m)}E_{\text{TED}}^{(m)*}$ are negligible; thus, Eq. (S18) is simplified to

$$\begin{aligned}\Delta\bar{I}_{\text{inter}}^{(m)} &= \frac{\sum_{n=1}^{N}\left[2\text{real}\left(E_{\text{TE}}^{(m)}E_{\text{ref}}^{*}+E_{\text{TES}}^{(m)}E_{\text{TED}}^{(m)*}+E_{\text{TED}}^{(m)}E_{\text{ref}}^{*}\right)\big|_{t=(4n-3)/(4f_{\text{mod}})}\right]}{N} \\ &\quad - \frac{\sum_{n=1}^{N}\left[2\text{real}\left(E_{\text{TE}}^{(m)}E_{\text{ref}}^{*}+E_{\text{TES}}^{(m)}E_{\text{TED}}^{(m)*}+E_{\text{TED}}^{(m)}E_{\text{ref}}^{*}\right)\big|_{t=(4n-1)/(4f_{\text{mod}})}\right]}{N}\end{aligned} \tag{S19}$$

Across different cycles, $E_{\text{TED}}^{(m)}E_{\text{ref}}^{*} + E_{\text{TES}}^{(m)}E_{\text{TED}}^{(m)*}$ changes randomly, while $E_{\text{TE}}^{(m)}E_{\text{ref}}^{*}$ changes periodically following the illumination modulation. Thus, Eq. (S19) can be rewritten as

$$\begin{aligned}\Delta\bar{I}_{\text{inter}}^{(m)} &= \frac{\sum_{n=1}^{N}\left[2\text{real}\left(E_{\text{TES}}^{(m)}E_{\text{TED}}^{(m)*}+E_{\text{TED}}^{(m)}E_{\text{ref}}^{*}\right)\big|_{t=(4n-3)/(4f_{\text{mod}})} - 2\text{real}\left(E_{\text{TES}}^{(m)}E_{\text{TED}}^{(m)*}+E_{\text{TED}}^{(m)}E_{\text{ref}}^{*}\right)\big|_{t=(4n-1)/(4f_{\text{mod}})}\right]}{N} \\ &\quad + \left[2\text{real}\left(E_{\text{TE}}^{(m)}E_{\text{ref}}^{*}\right)\big|_{t=(4n-3)/(4f_{\text{mod}})} - 2\text{real}\left(E_{\text{TE}}^{(m)}E_{\text{ref}}^{*}\right)\big|_{t=(4n-1)/(4f_{\text{mod}})}\right]\end{aligned} \tag{S20}$$

After averaging over N cycles, the amplitude of the first term on the right-hand side of Eq. (S20) is reduced by a factor of $\sqrt{N}$. Therefore, by averaging over multiple illumination modulation cycles, the impact of the fast motions in scattering media is minimized.

Note S4. Curvature compensation and pixel matching.

The curvature of the DMD was compensated for to minimize wavefront error during playback step. As sketched in fig. S2A, we built a curvature measurement setup based on the existing DOPC system. First, all the DMD pixels were set to the “on” position. The transmitted beam (green open arrows) through PBS2 was modulated and reflected by the DMD. The beam (yellow

stealth arrows) reflected by PBS2 was again reflected by mirror M5, serving as a reference beam in the curvature measurement. The two beams were combined by BS1, and then passed through a 4*f* configuration (lenses L4 and L5) together and formed an interference pattern $I_{\mathrm{curv1}}(x, y)$ on the camera, which was conjugate with the DMD. Second, all the DMD pixels were set to the "off" position, and the intensity distribution $I_{\mathrm{curv2}}(x, y)$ of the reference beam was captured. Third, the binary wavefront distortion due to the curvature of the DMD was computed as

$$\varphi_{\mathrm{curv}}(x, y) = \begin{cases} 0, & I_{\mathrm{curv1}}(x, y) \geq I_{\mathrm{curv2}}(x, y) \\ \pi, & I_{\mathrm{curv1}}(x, y) < I_{\mathrm{curv2}}(x, y) \end{cases} \tag{S21}$$

Thus, the displayed binary amplitude map $D_{\mathrm{DMD}}(x, y)$ was compensated for as follows

$$D'_{\mathrm{DMD}}(x, y) = \begin{cases} D_{\mathrm{DMD}}(x, y), & \varphi_{\mathrm{curv}}(x, y) = 0 \\ 1 - D_{\mathrm{DMD}}(x, y), & \varphi_{\mathrm{curv}}(x, y) = \pi \end{cases} \tag{S22}$$

Mapping between the camera pixels and DMD pixels needed to be determined. Since the reflected light from the DMD did not fall on the camera in our design (Fig. 2A), we added an additional system (sketched in fig. S2B) to align the camera and determine the lookup table, which mapped the DMD pixels to the camera pixels. A pattern displayed by the DMD was relayed to mirror M6 via a 4*f* configuration (lenses L4 and L5) along the yellow stealth arrows and then reflected by M6. The reflected pattern was again relayed by the 4*f* configuration to the camera. We fine-tuned the positions of both mirror M6 and the camera to ensure that the DMD, mirror M6 and camera were exactly conjugate with each other. To achieve so, we added several markers on mirror M6 and adjusted both mirror M6 and the camera to correct positions so that the camera could clearly image the pattern displayed by the DMD and the markers on mirror M6 simultaneously. Then, some points with known positions were displayed by the DMD. By reading their positions on the camera, the lookup table from the DMD to the camera was calculated via interpolation.

Note S5. SNR of the averaged differential hologram.

The binary amplitude map displayed by the DMD was calculated by taking the difference of two averaged holograms $\bar{I}_{\text{inter1}}(x, y)$ and $\bar{I}_{\text{inter2}}(x, y)$. The SNR of $\bar{I}_{\text{inter1}}(x, y) - \bar{I}_{\text{inter2}}(x, y)$ affected the PBR of the time-reversed focus inside scattering media. In experiments, the GePGS was modulated for N cycles, and the two holograms $I_{\text{inter1}}^{(n)}(x, y)$ and $I_{\text{inter2}}^{(n)}(x, y)$ were captured in the n-th cycle. Thus, for a point at (x, y), the corresponding signal in the n-th cycle was

$$s^{(n)}(x, y) = I_{\text{inter1}}^{(n)}(x, y) - I_{\text{inter2}}^{(n)}(x, y) \tag{S23}$$

Thus, the mean of $s^{(n)}(x, y)$ over N cycles was

$$\mu(x, y) = \left|\sum_{n=1}^{N} s^{(n)}(x, y)/N\right| \tag{S24}$$

and the standard deviation of $s^{(n)}(x, y)$ was

$$\sigma(x, y) = \sqrt{\sum_{n=1}^{N}[s^{(n)}(x, y) - \mu(x, y)]^2/(N-1)} \tag{S25}$$

The SNR at point (x, y) is defined as

$$\text{SNR}(x, y) = \frac{\mu(x, y)}{\sigma(x, y)} \tag{S26}$$

Accordingly, the SNR of $\bar{I}_{\text{inter1}}(x, y) - \bar{I}_{\text{inter2}}(x, y)$ was calculated as

$$\text{SNR} = \frac{\sum_{y=1}^{N_y}\sum_{x=1}^{N_x}\text{SNR}(x, y)}{N_x N_y} \tag{S27}$$

where N_x and N_y are the total number of pixels in the horizontal and vertical directions.

Note S6. Filtering out the photons tagged by the GePGS from noise photons.

For living tissue, both fast decorrelation components due to blood flow and slow decorrelation components due to other motions induce noise during the process of OPC. To filter out the photons tagged by the GePGS from noise, the frequency lock-in method was utilized while the GePGS was modulate for *N* cycles. The signal enhancement of the tagged photons over *N* cycles is defined as

$$R_{\text{enhance}}(N) = \frac{\sum_{m=1}^{M}\left|\int_0^{N/f_{\text{mod}}} I_{\text{with}}^{(m)}(t)\exp(-i2\pi f_{\text{mod}}t)dt\right|}{\sum_{m=1}^{M}\left|\int_0^{N/f_{\text{mod}}} I_{\text{without}}^{(m)}(t)\exp(-i2\pi f_{\text{mod}}t)dt\right|} \tag{S28}$$

where, $I_{\text{with}}^{(m)}(t)$ and $I_{\text{without}}^{(m)}(t)$ denote the intensities of the *m*-th pixel with and without GePGS modulation, respectively, and *M* denotes the total number of pixels of the camera.

To study the relationship between the signal enhancement of the tagged photons and the total cycle number *N*, *in vitro* experiments were conducted. The phantom was made by sandwiching DrBphP-PCM (~300 μM) based GePGS and a tube filled with 1% intralipid solution between two ground glass diffusers (DG-120, Thorlabs), as illustrated in fig. S4A. The intralipid solution inside the tube was pumped by a syringe with a specific flow speed v_t to adjust the fast decorrelation time τ_{c_fast}. One of the ground glass diffuser was moved by a linear translation stage with a specific translating speed v_g to adjust the slow decorrelation time τ_{c_low}. Three sets of experiments were performed: (1) intralipid pumping only to mimic a scattering medium containing a fast decorrelation component only. The speckle correlation coefficient curve is plotted in fig. S4B, where the decorrelation time is τ_{c_fast} = 7.5 ms; (2) intralipid pumping and diffuser translation to mimic a scattering medium containing both fast and slow decorrelation components. The speckle correlation coefficient curve is plotted in fig. S4C, where the fast decorrelation time τ_{c_fast} = 7.5 ms and the low decorrelation time is τ_{c_slow} = 9.5 s; (3) no pumping or translation to mimic a static scattering medium. The signal enhancements of the tagged photons for the three cases are shown in fig. S4D. It can be observed that the signal enhancement of the static scattering medium is the highest, while the signal enhancement of the scattering medium with both fast and slow decorrelation is the lowest.

Supplementary Figures:

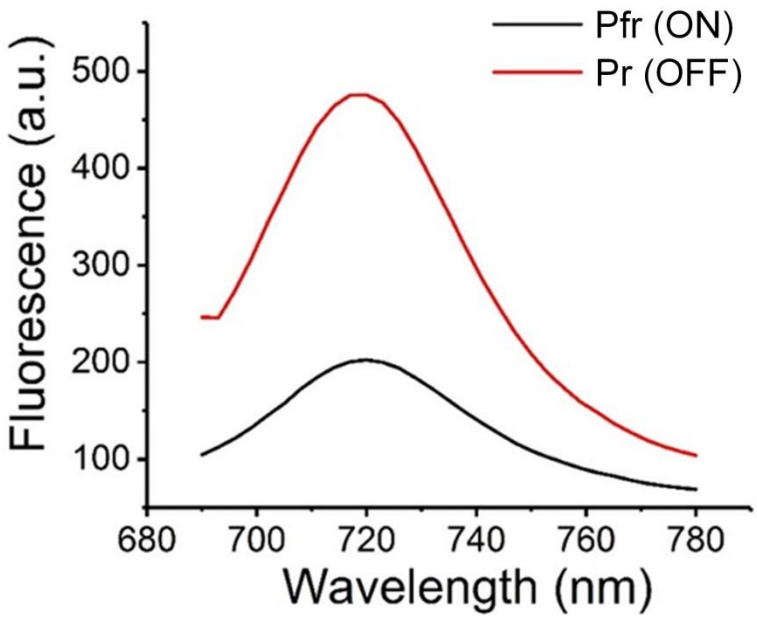

Fig. S1. Fluorescence spectra of DrBphP-PCM in the Pr state (OFF; red line) and after photoconversion to the Pfr state (ON; black line). Fluorescence of DrBphP-PCM was excited at 680 nm.

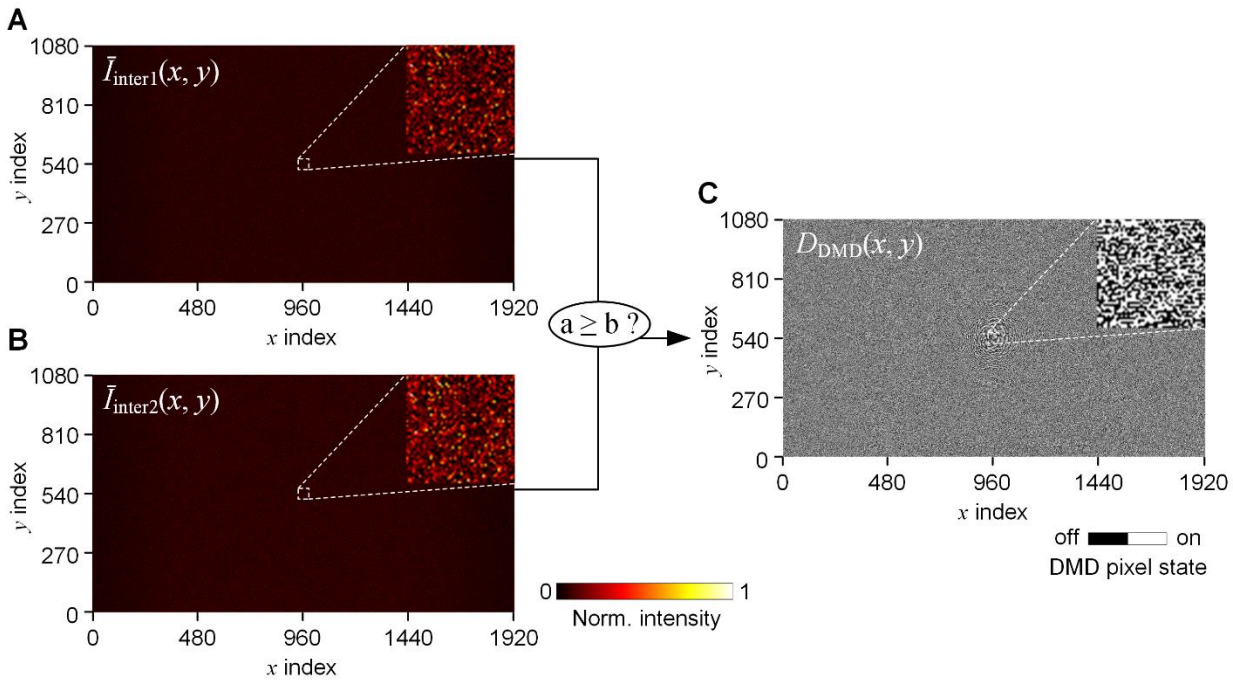

Fig. S2. Calculation of the binary amplitude map displayed on the DMD. (**A** and **B**) Two averaged holograms $\bar{I}_{inter1}(x, y)$ and $\bar{I}_{inter2}(x, y)$ captured with a time interval of 25 ms during the process of switching GePGS off. (**C**) Calculated binary amplitude map $D_{DMD}(x, y)$ displayed on the DMD.

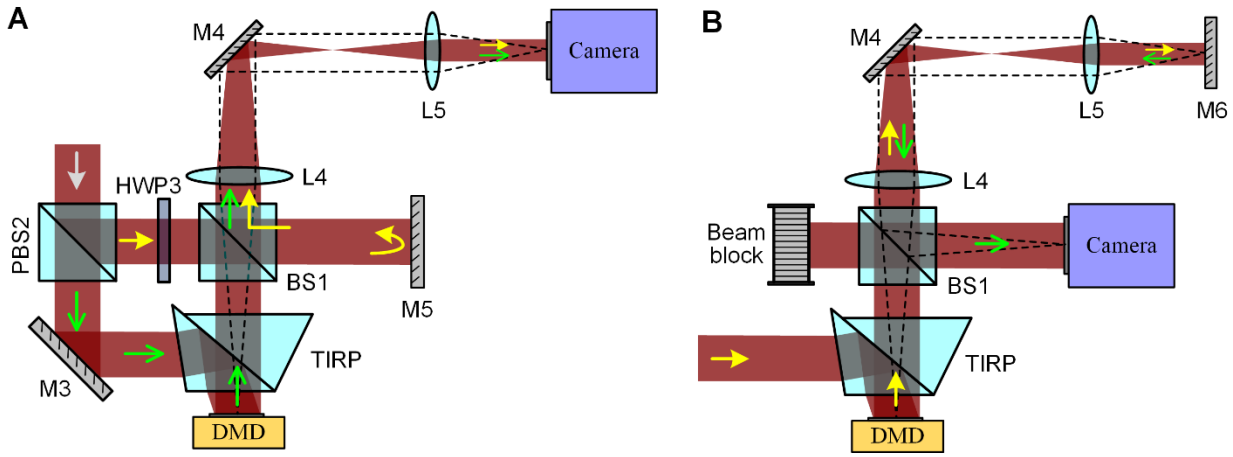

Fig. S3. DMD curvature compensation and pixel matching between the DMD and the camera. (**A**) DMD curvature measurement and compensation setup. (**B**) Setup for camera alignment and pixel matching. HWP, half wave plate; PBS, polarizing beam splitter; M, mirror; L, lens; BS, beam splitter; TIRP, total internal reflection prism; DMD, digital micromirror device.

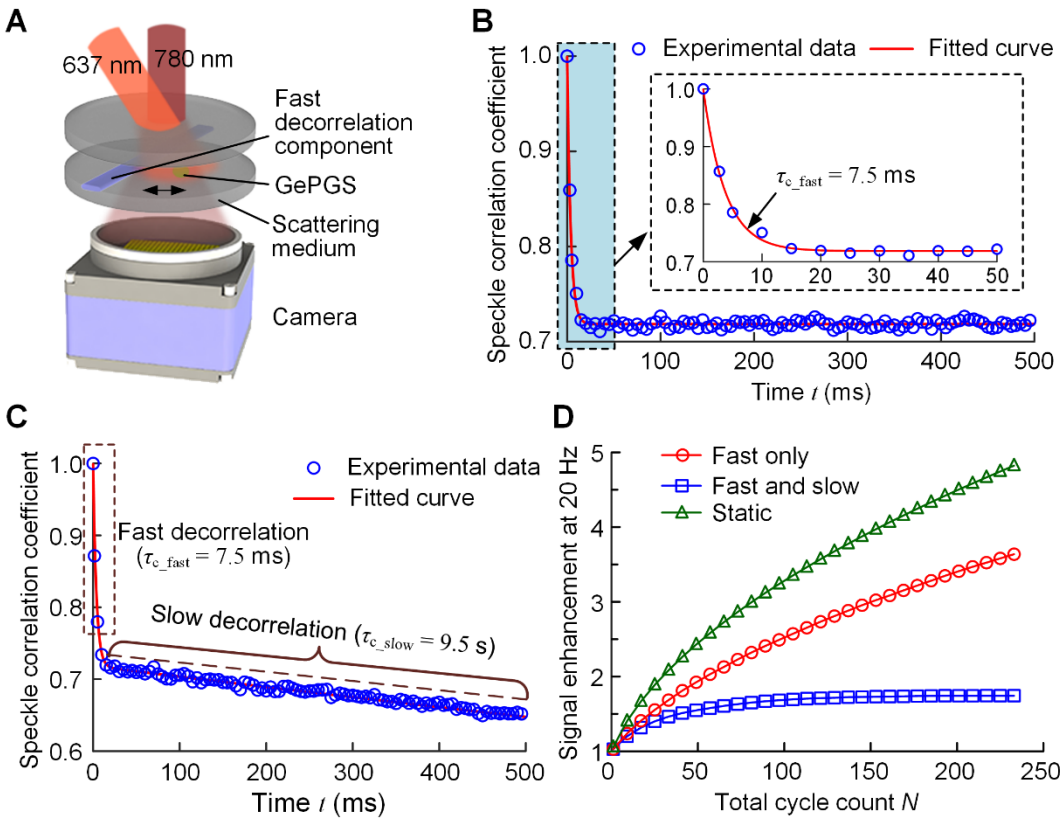

Fig. S4. Relationship between the detected signals of tagged photons and the total cycle number. (**A**) Experimental setup. (**B**) Speckle correlation coefficient as a function of time t for a scattering medium containing a fast decorrelation component only with a decorrelation time τ_{c_fast} of 7.5 ms. (**C**) Speckle correlation coefficient as a function of time t for a scattering medium containing both fast and slow decorrelation components. The decorrelation time of the fast decorrelation component τ_{c_fast} is 7.5 ms, while the decorrelation time of the slow decorrelation component τ_{c_slow} is 9.5 s. (**D**) Comparison of the signal enhancements of tagged photons (at 20 Hz) as a function of the total cycle count N for the scattering media containing a fast decorrelation component only, both fast and slow decorrelation components, and static component (no decorrelation at all).

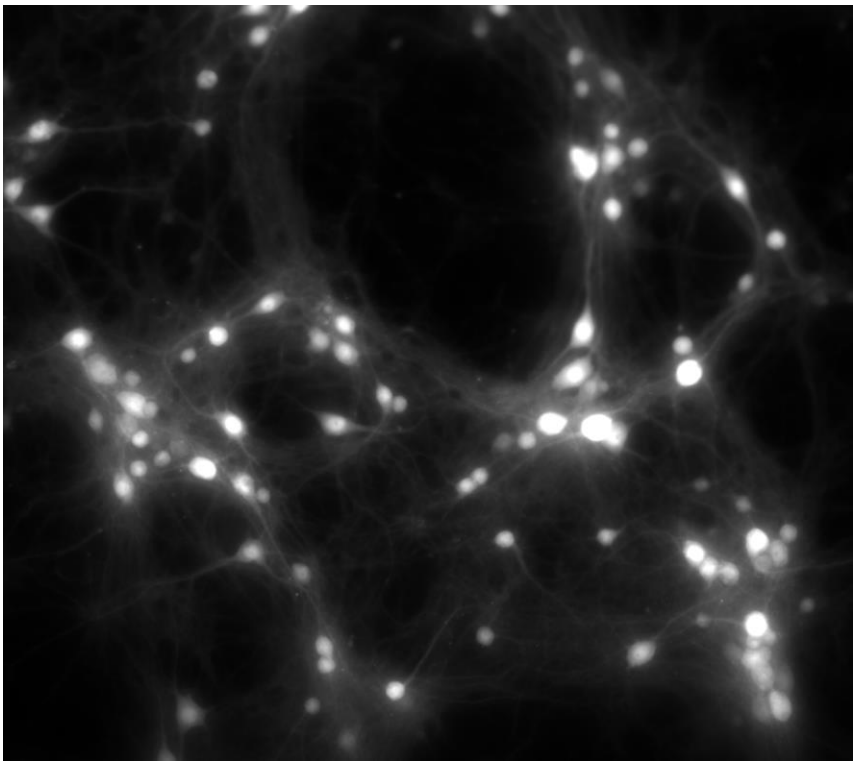

Fig. S5. Fluorescence imaging of DrBphP-PCM in live neurons. Murine hippocampal primary cultured neurons were transduced with 10^{10} viral genomes per well in a 24-well plate on day 10 *in vitro* and imaged on day 14 *in vitro*. Excitation filter was 620/15 nm, emission filter was 725/50 nm.

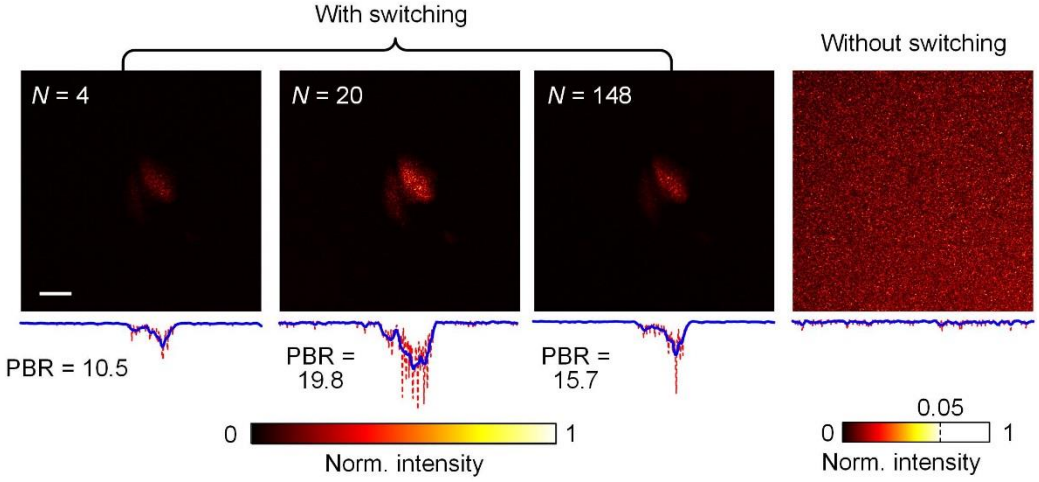

Fig. S6. Normalized intensity distribution of the optical foci inside the brain slices. Left, with 637-nm light switching for N = 4, 20 and 148, respectively; right, without 637-nm light switching. Scale bar, 100 μm.